RSC Advances

PAPER

View Article Online
View Journal | View Issue

Cite this: *RSC Adv.*, 2022, **12**, 33945

UV-curable self-matting waterborne polyurethane acrylate coating *via* self-wrinkled surface during curing in open-air

Haiqiao Zhang [a] and Zhihui Wu *[ab]

Received 23rd September 2022
Accepted 22nd November 2022

DOI: 10.1039/d2ra06010h

rsc.li/rsc-advances

This study developed and evaluated a series of ultraviolet (UV) curable self-matting waterborne polyurethane acrylate (UV-WPUA) coatings based on the self-wrinkled surface during UV-curing in the open-air. This method is simple, efficient, eco-friendly, and it does not require complicated or expensive equipment. The FT-IR spectrum indicates that the peaks of C=C in UV-WPUA have disappeared after UV irradiation. The gloss value of the UV-WPUA cured film can be affected by the wrinkles on the surface of the film and adjusted it by controlling the content of the photoinitiator in the liquid coating, since the content influences the dimensions of the wrinkles. As the height of the wrinkle increased, the gloss value of the UV-WPUA cured film decreased, and when the incident angles are 20° and 60°, the gloss values are less than 3 GU and 5 GU, respectively. Moreover, the cured film has a maximum water contact angle of 109°, which is affected by wrinkles and positively correlated with the surface roughness of the film. Furthermore, the cured film has excellent properties of thermal stability, tensile strength, pencil hardness, cross-cut adhesion and resistance to abrasion properties, making it well suited for the furniture, leather, and textile applications.

1. Introduction

As a type of functional surface decoration coating, matte coatings have been applied to leather finishing,[1] vehicle interior topcoats,[2] paper,[3] textiles,[4] and wood finishing.[5] The matte coating is generally prepared using three different strategies. The first strategy involves adding matting agents to the coating, the second involves developing self-matting resins, and the third is the physical extinction of the coating surface. In fact, all of the methods aim to produce a surface that is rough to a certain degree and low gloss.[6,7]

For the first strategy, various matting agents have been widely applied by coating industrial production,[8,9] including diatomite,[10] silica,[11] montmorillonite,[12] and clay. A rough surface is obtained after the powder is deposited on the surface of the coating. Due to the incompatibility[13] of the matting agents with organic resins and precipitation problems in the coating layer, the matting agents may be difficult to disperse, reducing the mechanical properties of the cured coating film.[14] As for the self-matting resin, it is a chemical extinction method without any matting agents, and the rough surface is generated by the resin itself.[15] The objective of this strategy is to obtain large polymer particles by adjusting the weight ratio of hard/soft monomers,[16] and introducing hydrophilic units.[17] Once the coating has been cured, these large particles could be deposited on the coating layer, resulting in a rough surface and low gloss.[18]

In terms of the third strategy, the vacuum UV and oxygen-free environment (typically nitrogen) are required for the generation of wrinkles on the coating surface. This method is complex and expensive in terms of equipment. During the vacuum UV irradiation, the coating is firstly only pre-cured on its surface layer. During the subsequent curing process, the stress caused by the depth gradient cured polymer is transmitted to the thin cured surface layer, which releases the stress as wrinkles.[19–21] In order to prevent the relaxation of stresses at the film surface, UV-LED or mercury lamp are required for subsequent irradiation to maintain the wrinkles. The wrinkles are arranged in a disorderly manner and have a micro–nano scale height and wavelength, which leads to a low gloss of the coating surface. Furthermore, an approach proposed by Chandra and Crosby[22] provides a method for the preparation of self-wrinkled polymer films that can be cured by an open-air mercury lamp. The oxygen inhibition prevented the top layer of liquid resin from curing, whereas the inner layer formed a gradient crosslinked film. The gradient crosslinked film was swollen by the liquid resin layer, which resulted in wrinkles. This method has been in-depth investigated by Lacombe and Soulié-Ziakovic,[23] including the balanced competition between oxygen inhibition and polymerization rates as a crucial factor.

[a]College of Furnishings and Industrial Design, Nanjing Forestry University, Nanjing 210037, Jiangsu, China. E-mail: wzh550@sina.com
[b]Jiangsu Co-Innovation Center of Efficient Processing and Utilization of Forest Resources, Nanjing 210037, Jiangsu, China

With the increasing awareness of environmental protection has increased the promotion of green production in the manufacturing industry.[24–26] Waterborne UV-curable coatings have gained popularity as combine the advantages of both waterborne and UV-curing technology. To reduce the viscosity of the oligomer, this type of coating utilizes water as the diluent. Furthermore, it features the characteristics of "5E",[27] low VOCs, and eco-friendly.[28–30] The cured film obtained by UV-curable coating is usually high gloss,[31] and the matte surface is rarely reported. To the best of our knowledge, no studies have been conducted on UV-curable self-matting waterborne coatings *via* self-wrinkled surfaces during open-air curing.

Herein, a series of UV-curable self-matting waterborne polyurethane acrylate (UV-WPUA) coatings were prepared based on the self-wrinkled surface during UV irradiation in open-air with the mercury lamp. The self-matting characteristic is due to its self-wrinkled surface, without using any matting agent, complicated or expensive equipment such as an excimer lamp, or nitrogen equipment. The self-matting UV-WPUA coating is coated on the wood substrate in this study, and its application performance is evaluated.

2. Experimental section

2.1 Materials

During the experiments, the following starting materials were used: UV-WPUA oligomer (JZ-4234) was obtained from Nanjing Jiazhong Chemical Technology Co., Ltd in Nanjing, China. The Photoinitiator 819DW (a dispersion of bis-acylphosphine oxide (BAPO) in water) was supplied by Shanghai Yinchang new material Co., Ltd in Shanghai, China. Defoamer (SRE-2020), dispersant (SRE-4190), and leveling additives (SRE-3251) were bought from Guangzhou Dong Prosperous Chemical Raw Materials Co., Ltd in Guangzhou, China. The fillers talcs powder (8 μm) and silicon dioxide (SiO_2, the particle size is about 1 μm) were obtained from Hebei Yonghua Wear Resistant Materials Co., Ltd in Xingtai, China. A UV-curable commercial priming coating (A185721006) was supplied by the Dazbole Polymer Material Co., Ltd in Hangzhou, China. Water used in this study was prepared by the Plus-E3-10th ultra-pure water Machine (EPED, Nanjing, China). All the materials were utilized as received without purification.

2.2 Synthesis of UV-WPUA coatings

The formulas of UV-WPUA coatings were following Table 1. The UV-WPUA oligomer was first mixed with the defoamer at 500 rpm for 10 min using a disperser (SDF-450, Qiwei, Hangzhou, China). Every remaining component was sequentially homogenized at 1000 rpm for 10 min, resulting in a uniform UV-WPUA coating. The SiO_2 in C_3 is used as a wear-resistant filler, not a matting agent.

2.3 Preparation of UV-WPUA films

The UV-curable commercial primer coating was cured on the wood substrate with irradiation of a mercury lamp and sanded with 240 grit sandpaper. Following this step, the UV-WPUA coating was coated on the primer coating-wood substrate by bar-coating method (the thickness of the wet film was about 120 μm). The UV-curing process was carried out using a UV mercury lamp, and the UV intensity was 6.6 mW cm^{-2} (measured by an LS132 UV energy meter, Linshang, Shenzhen, China). After 3 min of UV irradiation, the cured films were obtained and labeled by F_1, F_2, and F_3. The method of GB/T 1728-2020 was used to determine 100% polymerization of UV-WPUA oligomer in the presence of oxygen inhibition.

2.4 Instrument and characterization

2.4.1 Chemical structure characterization. The chemical structure and compositions of UV-WPUA oligomer, liquid coatings, and cured coating films were characterized on an FT-IR spectrometer (Vertex 80, Bruker, Germany) using the FTIR-ATR mode. The date was obtained with the wavenumbers between 4000 cm^{-1} and 400 cm^{-1} at a 0.5 cm^{-1} resolution. The acrylate conversion was determined by the CH_2═CH twisting peak area around 808 cm^{-1},[32] and the peak area at 1722 cm^{-1} (C═O stretching vibration) was employed as an internal standard peak.[33] The FTIR spectra of liquid coatings and cured coating films were analyzed using Thermo's Omnic software version 9.3, and the acrylate conversion was calculated using eqn (1)

$$\text{Conversion } (\%) = \left[1 - \frac{(A_{808}/A_{1722})_t}{(A_{808}/A_{1722})_0}\right] \times 100 \quad (1)$$

where $(A_{808}/A_{1722})_t$ and $(A_{808}/A_{1722})_0$ are respectively the relative absorption of the liquid coating and cured coating film after UV irradiation time (t).

2.4.2 Physical and mechanical properties characterization

2.4.2.1 Gloss. An HG268 gloss meter (3nh, Shenzhen, China) was used to measure the gloss value of cured film in accordance with GB/T 9754-2007 (ISO 2813:1994). The UV-

Table 1 Formulas of UV-WPUA coatings

Coating	Oligomer (g)	Defoamer (g)	Water (g)	Dispersant (g)	Leveling additive (g)	Photoinitiator (819DW, g)	Filler (g)
C_1	100.0	3.0	10.0	1.5	2.0	2.0	3.0 (talcs)
C_2	100.0	3.0	10.0	1.5	2.0	3.0	3.0 (talcs)
C_3	100.0	3.0	0	1.5	2.0	3.0	3.0 (SiO_2)

WPUA film was measured at eight different points using three different measurement geometries: at 20°, 60°, and 85°.

2.4.2.2 Roughness (R_a). The roughness of cured film was measured with the JB-4C precision roughness meter (Shanghai Precision Instruments Co., Ltd, Shanghai, China). The R_a was determined based on a measured length of 0.8 mm.

2.4.2.3 Water contact angle. A DSA100S (KRÜSS, Hamburg, Germany) drop-shape analyzer was used to evaluate the water contact angle of the cured film. For testing, the wood substrate (10 cm × 10 cm) with the cured film was sawed into 1 cm wide pieces. Each cured film was tested at 5 different positions, and the water contact angle at each position was recorded at different elapsed time (0 s, 5 s, 10 s, and 20 s).

2.4.2.4 Basic properties. The tensile strength of cured film was measured with an AGS-X electronic universal testing machine (Shimadzu, Kyoto, Japan). The samples were made into a dumbbell shape by a silica gel mold with the type of 1BA according to GB/T 1040.2-2006 (ISO 527-2:1993).

The properties of hardness (measured with BY-500g, Pushen, Shanghai, China), cross-cut adhesion (determined with QFH-A, Airuipu, Quzhou, China), and resistance to abrasion (measured with BGD-532 with CS-10 abrading rubber wheels, 500 g, 500 r, Biuged, Guangzhou, China) of the cured film were evaluated according to GB/T 6739-2006 (ISO 15184:1998), GB/T 4893.4-2013, and GB/T 1768-2006 (ISO 7784-2:1997), respectively.

2.4.3 Microscopy investigations. The morphologies of the cured film (surface and cross-section) were performed with a Quanta 200 scanning electron microscopy (SEM, FEI, Hillsboro, Oregon, USA). The cured film was attached to a copper sample table and deposited with an extremely thin gold layer, while the acceleration voltage was set at 15 kV for the observation. Furthermore, the surface topographies of the cured film were also observed using a Carl-Zeiss Imager Z1 microscope (Munchen, Germany) with AxioVision software using white light. The optical microscope (OM) images were collected at a magnification of 200×.

2.4.4 Thermogravimetric analysis (TGA). A TG 209F1 Libra thermogravimetric analyzer (Netzsch, Germany) was used to analyze the thermal behavior of cured films. The analysis was carried out under an N_2 flow of 50 mL min^{-1}, from 30 °C to 700 °C, at a heating rate of 10 °C min^{-1}. The measurement was taken using 4–5 mg powers of each cured film.

3. Results and discussion

3.1 Polymerization rate (R_p) *vs.* oxygen inhibition rate (R_{O2})

In this study, a series of UV-WPUA resins were used to analyze the balance condition between R_{O_2} and R_p. The additive and filler may affect the transparency of UV-WPUA oligomer, especially the solid filler, which can reduce UV propagation efficiency. When the efficiency of the photoinitiator (labeled by 819DW) is reduced, resulting in a decrease in the R_p of the UV-WPUA oligomer, thereby altering the balance condition between R_p and R_{O_2}. As a result, six UV-WPUA resins without other components were prepared, the concentrations of 819DW were 1.0%, 1.25%, 1.5%, 2.0%, 2.5%, and 2.75%. UV-WPUA resins were cured with two different UV intensities, *i.e.*, 16.1 mW cm^{-2} (distance from UV lamp about 15 cm) and 6.6 mW cm^{-2} (distance from UV lamp about 50 cm). There is a glass substrate on which the wet films were coated, and the thickness of each film was approximately 120 μm. Fig. 1A shows the acrylate conversion of six UV-WPUA resins after irradiation for 3 min. Due to the oxygen inhibition, the top acrylate conversion of each film is lower than the bottom, and the acrylate conversion increases with increasing the concentration of 819DW. Regardless of whether the UV intensity is 16.1 mW cm^{-2} or 6.6 mW cm^{-2}, the lowest top acrylate conversion is from the film with a concentration of 819DW of 1.0%, and the lowest values under 16.1 mW cm^{-2} and 6.6 mW cm^{-2} are 62.4% and 44.1%, respectively. While the highest values of the top conversions occurred at an 819DW concentration of 2.75%, which are about 85%. The bottom acrylate conversion also follows a similar trend, where a higher UV intensity induces a higher acrylate conversion. As the concentration of 819DW increased, the effect of UV intensity on top and bottom acrylate conversion decreased. It is noted that when the concentration of 819DW is 1.0%, the top acrylate conversion of the film obtained by 16.1 mW cm^{-2} and 6.6 mW cm^{-2} is with a difference of 18.3%, while when the concentration of 819DW is 2.75%, the difference is just 0.1%. Similarly, the difference in the conversion of 819DW at two

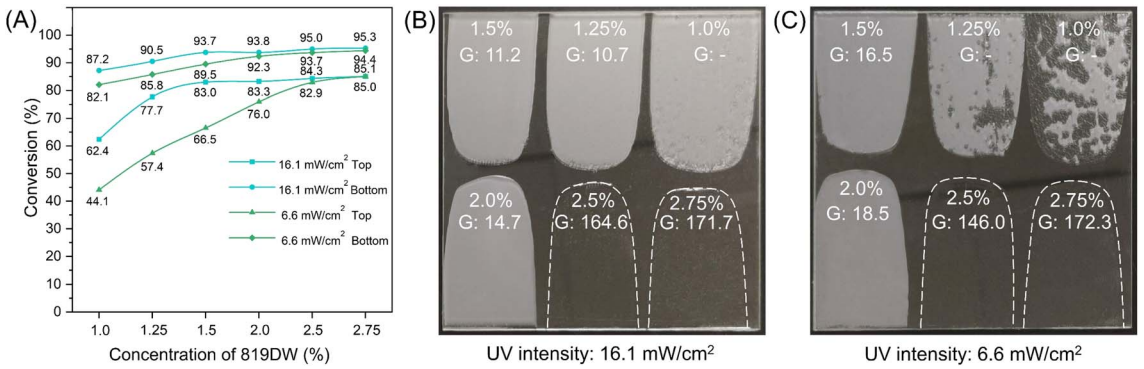

Fig. 1 (A) The top and bottom acrylate conversions of UV-WPUA resins under UV irradiation (3 min) at UV intensity of 16.1 mW cm^{-2} and 6.6 mW cm^{-2}; photos of UV-WPUA films taken after 3 min of UV irradiation at (B) 16.1 mW cm^{-2} and (C) 6.6 mW cm^{-2}, *G*: gloss value at 60°.

different UV intensities decreased from 5.1% to 0.9% as the 819DW concentration increased from 1.0% to 2.75%.

The photographs in Fig. 1B and C depict UV-WPUA films after UV irradiation for 3 min. It was found that the UV film was not completely cured when the UV intensity was 16.1 mW cm^{-2} and the UV-WPUA resin with an 819DW concentration of 1.0%, and the surface exhibited some sticky areas. The matte films (as can be seen from the gloss values at 60°) with a wrinkled surface have been obtained when the concentration of 819DW are 1.25%, 1.5%, and 2.0%. The film with a smooth, high gloss surface have been obtained with 819DW concentrations of 2.5% and 2.75%. In the presence of a UV intensity of 6.6 mW cm^{-2}, the UV-WPUA resin with 819DW concentrations of 1.0% and 1.25% could not be completely cured, resulting in the sticky surface. The concentrations of 819DW are 1.5% or 2.0%, which produce matte films; and 2.5% or 2.75%, which produce smooth, high gloss films.

Fig. 2A illustrates the mechanism of self-wrinkling of UV-WPUA resin. As the photoinitiator 819DW is irradiated with UV light, radicals are produced and reacted with the C=C in the WPUA oligomer, resulting in crosslinking and curing of the film. The oxygen in the air, however, would react with the radical (R$^{\bullet}$) and produce R–O–O$^{\bullet}$, which would trap the radical.[34] As a result, it reduces the acrylate conversion in the top thin layer of the UV-WPUA oligomer, resulting in the creation of a liquid layer[35] at the top of the UV-WPUA resin. It is almost impossible for the oligomer beneath the top liquid layer to be affected by oxygen and can crosslink to the film. Furthermore, the liquid layer on the resin surface will cause the cured film to swell. Surface wrinkles are generated when the difference in osmotic pressure between two parts is significant enough.[36] This phenomenon appears to occur as a result of the balanced competition between R_p and R_{O_2} of UV-WPUA resin, *i.e.*, $R_p \approx R_{O_2}$, as described by Lacombe and Soulié-Ziakovic.[23] A completely cured and smooth surface is obtained when R_p is greater than R_{O_2}, such as the films with 819DW contents of 2.5% and 2.75% in Fig. 1B and C; while R_p is less than R_{O_2}, UV-WPUA could not be completely cured, resulting in a sticky surface.

As can be seen in the OM images of the obtained films in Fig. 2B, by combining Fig. 1B and C, there are wrinkles on the surface of the incompletely cured film, and cracks (see orange arrows) appear in the sticky area. In the case of completely cured films, there are two types: one has random wrinkles and low gloss; the other has smooth surfaces, no wrinkles, and high gloss.

As evidenced in our study, UV-WPUA resin with the 819DW concentrations of 1.5% to 2.75% could be completely cured with the UV intensity was 6.6 mW cm^{-2}. In the presence of a higher UV intensity (16.1 mW cm^{-2}), UV-WPUA resin with the 819DW concentration of 1.25% can also be completely cured. It is important to note that at the high UV intensity curing position the UV mercury lamp is situated too close (approximately 15 cm) to the resin surface, and the temperature is up to about 100 °C, which may cause damage to some substrates (such as wood and leather). Therefore, in this study, the coating was cured under a UV intensity of 6.6 mW cm^{-2}. As described above, the additives and fillers may affect R_p of UV-WPUA coating. Therefore, the 819DW content in the formulations of UV-WPUA coatings in "2.2 Synthesis of UV-PUA coatings" is different from that of UV-WPUA resin. According to our study, the UV-WPUA coatings contain the additive, filler, and diluent (water), and the 819DW content could be greater than 2.5% without producing a smooth and high gloss surface.

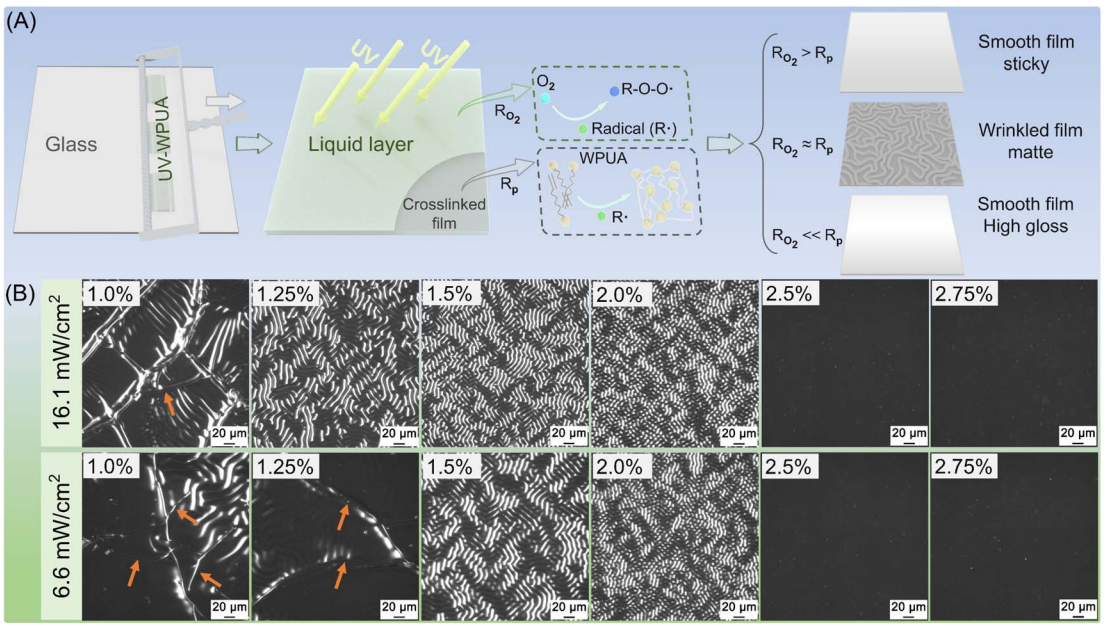

Fig. 2 (A) The mechanism of the self-wrinkled surface of UV-WPUA film during cured in the open-air, (B) the OM images of UV-WPUA films obtained with two different UV intensities.

3.2 Chemical structure

The chemical structure of liquid UV-WPUA coatings and cured coating films were analyzed by the FT-IR spectra (Fig. 3). It has been found that the characteristic peaks of C=C vibrations at 1634, 1407, and 808 cm^{-1} disappeared after UV irradiation (red areas),[37] indicating that the radicals were reacted with C=C bonds in liquid UV-WPUA coating. After UV irradiation, there is a new absorption peak that appeared at 1631 cm^{-1}, not the peak of C=C vibrations that appeared at 1634 cm^{-1} shifted to 1631 cm^{-1}, which was caused by the residual moisture in the cured coating films. The absorption bands at 3437 and 1631 cm^{-1} are ascribed to the O–H vibrations[38] of the residual moisture. The characteristic peaks at 2955 and 2870 cm^{-1} (WPUA oligomer and liquid coating) or 2924 and 2869 cm^{-1} (cured coating film) are assigned to the C–H stretching vibration in CH_2 and CH_3, while the peak at 1458 cm^{-1} is attributed to the C–H deformation vibration in CH_2 and CH_3.[39] There are absorption bands around 1720 (or 1722) and 1106 cm^{-1}, which correspond to the vibrations of –C=O and C–O–C vibration, respectively.

The characteristic peaks of C_1, C_2, and C_3 are consistent with most of the WPUA oligomer. Some of the peaks in the C_1, C_2, and C_3 differ from those in the WPUA oligomer as a result of the different additives and fillers added. In the spectra of F_1, F_2, and F_3, there was no C=C absorption peak after UV irradiation for 3 min. The acrylate conversions of C_1, C_2, and C_3 have been determined to be 67.8%, 75.1%, and 64.8%, respectively. During UV-curing, the fluidity of the polymer has a significant impact on the conversion efficiency. Since C_3 does not contain diluent (water), its viscosity is greater than that of C_1 and C_2. Due to the immobility of the acrylic group,[40] it may be difficult for the high viscosity system to cure completely, which is why the acrylate conversion of C_3 is lower than that of C_1 and C_2.

3.3 Gloss, micro-morphologies, and water contact angle

As shown in Fig. 4, with the incident angles of 20° and 60°, the gloss values of F_1, F_2, and F_3 differ slightly, and the gloss values

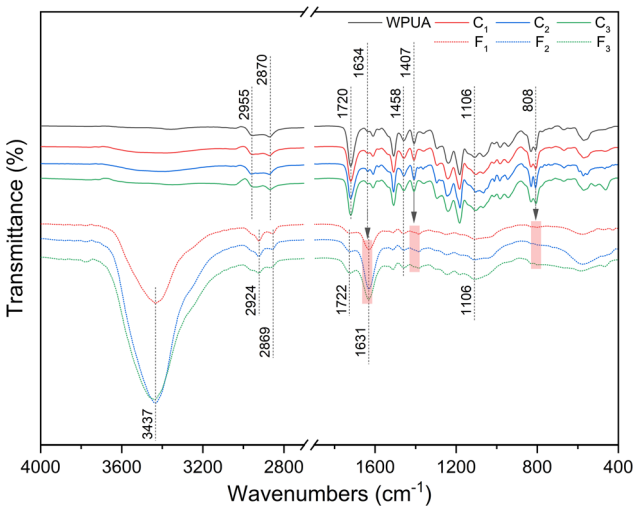

Fig. 3 The FT-IR spectra of WPUA oligomer, UV-WPUA coatings, and films.

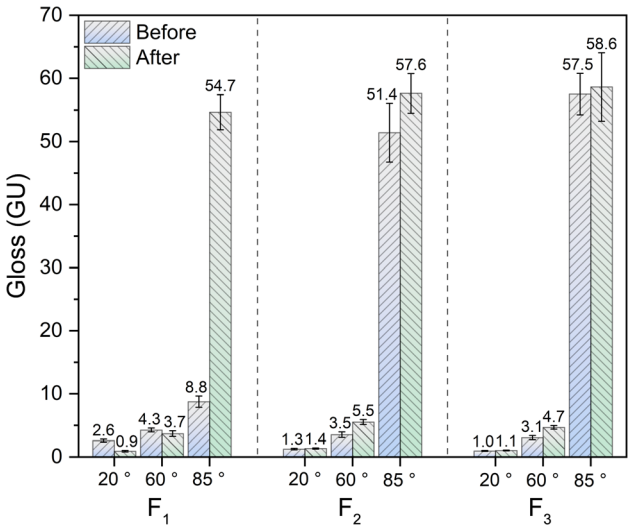

Fig. 4 The change in glosses of F_1, F_2, and F_3 after the resistance to abrasion test.

are less than 5 GU, satisfying the requirements of extinction classification.[41] In the case of an incident angle of 85°, the gloss values of F_2 and F_3 are 51.4 GU and 57.5 GU, respectively, while the gloss value of F_1 is 8.8 GU. Furthermore, after testing the

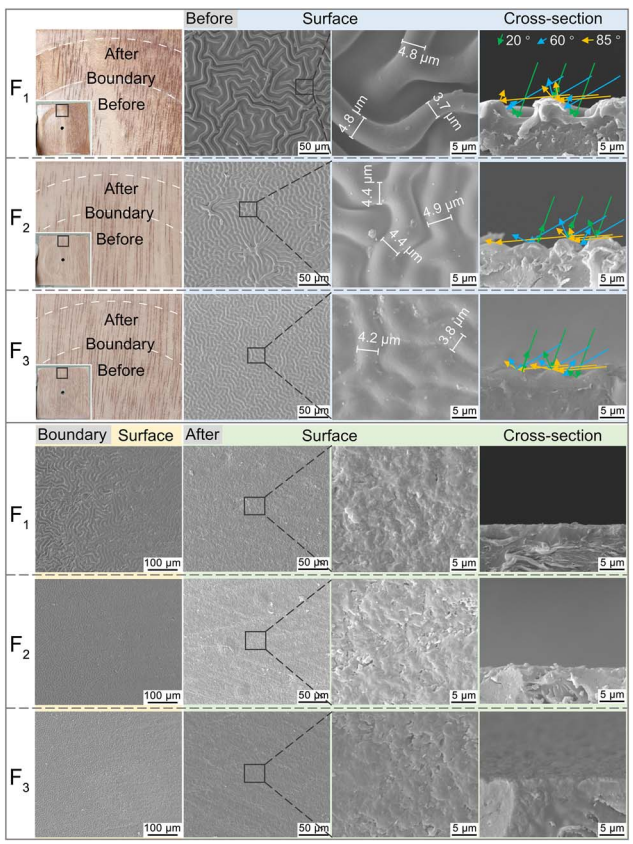

Fig. 5 The SEM images of F_1, F_2, and F_3 before and after the resistance to abrasion test, and the illustration of the self-matte mechanism based on the wrinkles.

resistance to abrasion property, the gloss value (85°) of F_1 increased to 54.7 GU.

The gloss value at 85° is a very important feature for matte coating film. The change of gloss is evident from the micro-morphologies[42,43] of the surface and cross-section of the cured coating film shown in Fig. 5, which shows photographs of the cured coating film and micro-morphologies of its surface and cross-section. On the surface of F_1, F_2, and F_3, the wrinkles with different dimensions are present. The width of wrinkles on the surface of the films varies from 3.7 μm to 4.9 μm, and the spacing between wrinkles in F_1 (9.53 μm) is greater than those of in F_2 (7.34 μm) and F_3 (6.10 μm). It is attributed to the fact that C_2 and C_3 contain more photoinitiator 819DW than C_1, as a result, more photoinitiators lead to denser wrinkles[44] and higher matting efficiency.[8,45] The gloss value of F_1 is much lower than those of F_2 and F_3 with the incident angle of 85°. The reason is that the height and spacing of wrinkles in F_1 surface are higher than those in F_2 and F_3 (Fig. 5), which causes incident light to be reflected or "captured" by the interspace of wrinkles. Further, the light received by the gloss meter acceptor is smaller, which results in a lower gloss.[42] As mentioned above, after testing for resistance to abrasion property, the gloss values at 85° in F_1, F_2, and F_3 increased. The SEM images in the low part of Fig. 5 indicate that some wrinkles still exist in the boundary section on the left and the wrinkles in the right region have been eliminated. The SEM images of the cross-section of the film showed that the wrinkles on the surface have disappeared after the test, the surface has become smoother, and the gloss value at 85° has increased as a result of the destruction of wrinkles.

An illustration of the water contact angles for UV-WPUA cured films with the different elapsed time (0 s, 5 s, 10 s, and 20 s) is shown in Fig. 6. It is identified that the initial water contact angles for F_1, F_2, F_3, and F_{ctrl} are 109.5°, 93.9°, 95.6°, and 61.6°, respectively. As the elapsed time increased, the water contact angles gradually decreased. F_1 has an initial water contact angle that is 15.6° larger than F_2, 13.9° larger than F_3, and 47.9° than F_{ctrl}. Among the films, the water contact angle of F_{ctrl} is the smallest, which does not meet the hydrophobic requirement (>90°). The water contact angles of the other three films are all above 90°, which are hydrophobic surfaces. The water contact angle is generally related to micro–nano structures[46–49] and the roughness of the film surface.[50] The R_a of F_1, F_2, and F_3 are 0.35 μm, 0.22 μm, and 0.25 μm, respectively (as shown in Fig. 6). The F_{ctrl} is a smooth, high gloss film with a minimum roughness of 0.11 μm. According to the Wenzel wetting model, the water contact angle increase with increasing surface roughness when the water contact angle exceeds 90°,[51] which explains the difference in the water contact angle of cured coating films.

3.4 Thermal stability

The thermal behavior of cured UV-WPUA coating film was analyzed by using TGA and derivative weight loss (DTG) curves, as shown in Fig. 7. To further investigate the degradation

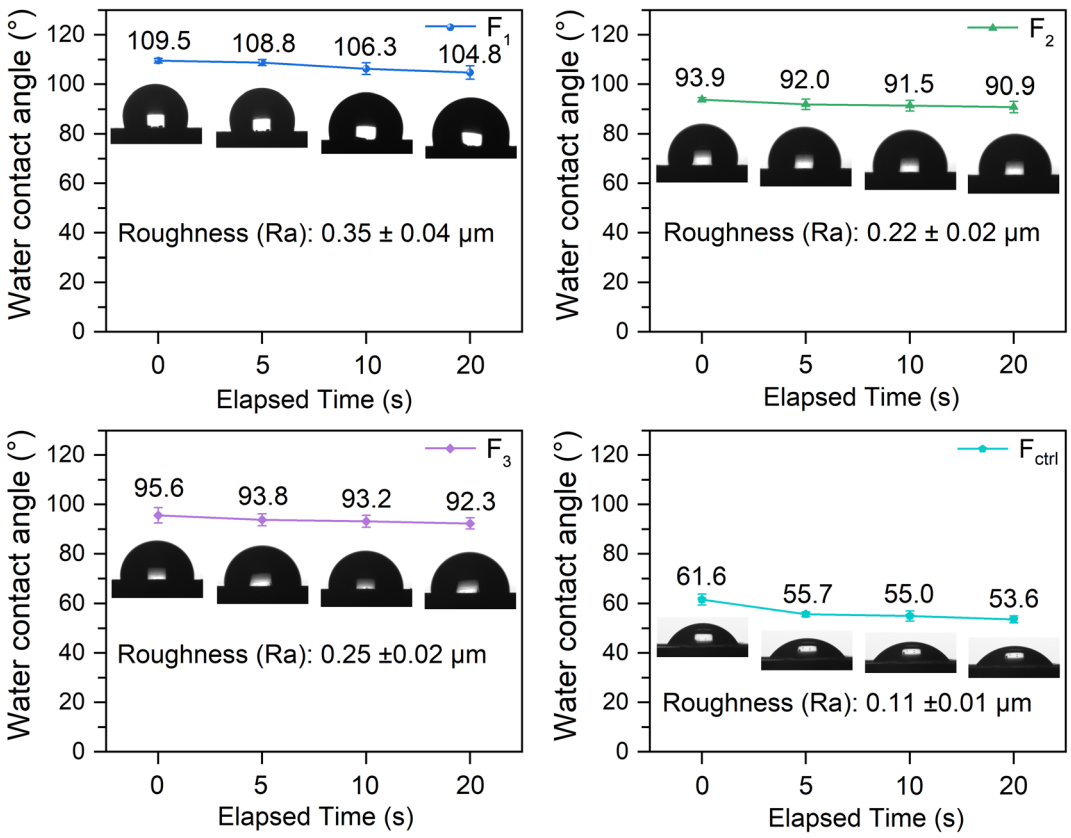

Fig. 6 The water contact angle of F_1, F_2, F_3, and F_{ctrl} (film obtained by UV-WPUA + 3.0% 819DW) with the different elapsed time.

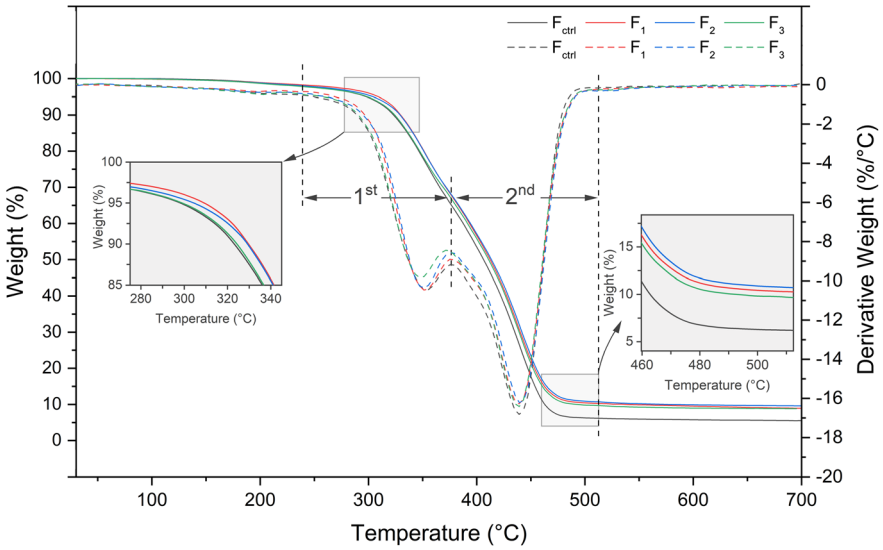

Fig. 7 TGA (solid) and DTG (dashed line) thermograms of UV-WPUA films.

behavior of these films, some specific data were recorded in Table 2. The first is the temperature of initial 5% and 50% mass loss, *i.e.*, $T_{5\%}$ and $T_{50\%}$; the second is residual mass percent at 700 °C, and the last is the maximum weight loss rate and corresponding temperature in the degradation stage.

It was observed that all the cured coating films showed a similar two-stage degradation process, with two main regions of weight loss, and the peaks were around 350 °C and 440 °C, respectively. From 239 °C to 375 °C, the first stage occurs, accompanied by a weight loss of 33% due to the urethane bonds in hard segments.[52] At 375 °C to 510 °C, the second stage appears, which is associated with a weight loss of about 57% (F_{ctrl} is about 61%), which corresponds to the decomposition of the soft segment of PUA.[53] As demonstrated by Fig. 7, cured UV-WPUA films degrade in the high-temperature regions more delayed than F_{ctrl}. At 700 °C, F_1, F_2, and F_3 have residues of 8.95%, 9.63%, and 8.81%, respectively, which are higher than F_{ctrl} (5.54%). A further observation is that the $T_{5\%}$ and $T_{50\%}$ of all the cured UV-WPUA films are delayed more than F_{ctrl}, which indicates that the cured UV-WPUA films are slightly more thermally stable than F_{ctrl}. According to these results, the additives and fillers can improve the thermal stability of the UV-WPUA films, consistent with the research findings of Ding *et al.*[4] Furthermore, F_2 shows the higher thermal stability than F_1 and F_3 based on the residual mass percent. As discussed in the "3.2 Chemical structure" section, the acrylate conversion of C_2 (75.1%) is higher than those of C_1 (67.8%) and C_2 (64.8%). A higher acrylate conversion results in a higher crosslinking density and improves the thermal stability of the film.[54] In view of the above, cured UV-WPUA films exhibit excellent thermal stability and higher thermal resistance than pure WPUA film.

3.5 Basic properties

The basic properties of UV-WPUA coating films are shown in Fig. 8. The pencil hardness of F_1 is *H*, whereas F_2 and F_3 have a pencil hardness of 2*H*, which is attributed to the higher content of the photoinitiator in C_2 and C_3 compared to C_1. In terms of the resistance to abrasion property, F_1 is slightly worse than F_2 and F_3, which are 0.049 g, 0.045 g, and 0.047 g, respectively. It is known that the acrylate conversion of C_2 is greater than those of C_1 and C_3, which induces higher crosslinking density, resulting in a slight improvement in the resistance to the abrasion properties of F_2. However, it is worth noting that the acrylate conversion of C_3 is lower than that of C_1, while the resistance to abrasion property and pencil hardness of F_3 is better than that of F_1. It seems to be in contradiction with the previously mentioned that high conversion rate and good mechanical properties of the films. Indeed, the reason is that the filler in C_3 is silica, and its mechanical properties are better than talcs[55] in F_1, which makes the mechanical properties of F_3 better than F_1. The tensile strengths of cured films are illustrated in Fig. 8B, the values of F_1, F_2, and F_3 are 19.28 ± 2.07 MPa, 24.60 ± 1.83 MPa, and 21.72 ±

Table 2 Pyrolysis parameters of UV-WPUA films

			1st deg. stage		2nd deg. stage		
Film	$T_{5\%}$ (°C)	$T_{50\%}$ (°C)	T_{max} (°C)	DTG_{max} (%/°C)	T_{max} (°C)	DTG_{max} (%/°C)	Residue (%)
F_{ctrl}	298.2	406.3	355.5	10.59	438.9	16.93	5.54
F_1	309.3	412.4	353.5	10.70	439.0	16.41	8.95
F_2	304.4	413.6	351.9	10.59	440.0	16.37	9.63
F_3	299.1	411.0	349.9	9.92	438.6	16.60	8.81

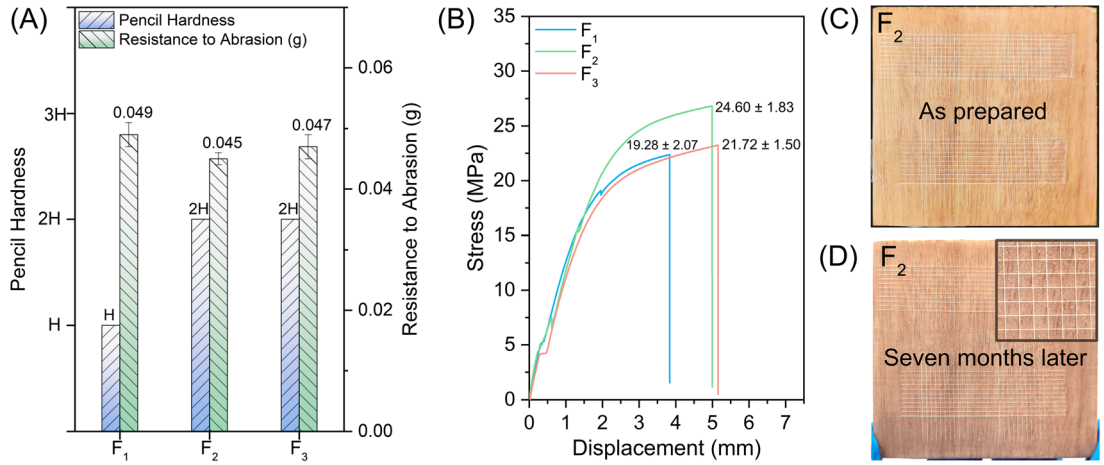

Fig. 8 (A) The pencil hardness and resistance to abrasion properties of cured films; (B) the tensile strength of cured films; the digital photos of F_2 after cross-cut adhesion property test (C) and seven months later stored in the ambient surrounding (D). (Inset) Enlarged image of the cross-cut section.

1.50 MPa, respectively. These results are consistent with the properties of wear resistance, that is, the tensile strength of F_2 is better than those of F_3 and F_1. In terms of cross-cut adhesion property, all films show the highest classification of level 0 (the optimal level, as shown in Fig. 8C and D). After seven months of storage in the ambient surrounding, the film (as exemplified by F_2) does not detach from the wood substrate.

4. Conclusions

We have demonstrated an approach to UV-curable self-matting WPUA coating based on the self-wrinkled surface during curing in the open-air. This method is simple, efficient, eco-friendly, and not requires complex or expensive equipment. After UV irradiation, the peaks of C=C in the WPUA oligomer disappeared in the FT-IR spectrum. The gloss value of the cured UV-WPUA coating film can be adjusted by modifying the formula of liquid UV-WPUA coating. By varying the photoinitiator content in the formula, different wrinkle dimensions can be achieved, and the gloss value can be varied accordingly. With the incident angle of 20°, the gloss value of the cured UV-WPUA film is less than 3 GU; and when the incident angle is 60°, the gloss value of the film is less than 5 GU; at 85°, the gloss was greatly affected by the wrinkle height, which decreased with increasing the height of wrinkle. Furthermore, the cured UV-WPUA film has a maximum water contact angle of 109°, which is positively correlated with the roughness of the wrinkled surface. In addition, the cured UV-WPUA film has excellent thermal stability and mechanical properties, which have great potential for practical applications in furniture, leather, and textile fields.

Conflicts of interest

The authors declare that they have no known competing financial interests or personal relationships that could have appeared to influence the work reported in this paper.

Acknowledgements

The authors thank the financial support from the National Key Research & Development Program of China (No. 2016YFD0600704, 2018YFD0600304) and the Postgraduate Research & Practice Innovation Program of Jiangsu Province (No. KYCX22_1095).

References

1 T. Xie, W. Kao, Z. Zhang, Y. Liu and Z. Li, Synthesis and characterization of organosilicon modified self-matting acrylate polymer: Insight into surface roughness and microphase separation behavior, *Prog. Org. Coat.*, 2021, **157**, 106300.
2 J. Uribe-Padilla, M. Graells-Sobre and J. Salgado-Valle, A novel contribution to the modeling of the matting efficiency of aqueous polyurethane dispersions, *Prog. Org. Coat.*, 2017, **109**, 179–185.
3 P. Samyn, J. Van Erps and H. Thienpont, Specular gloss versus surface topography for oil-filled nanoparticle coatings on paper, *Color Res. Appl.*, 2016, **6**(41), 596–610.
4 Z. Ding, J. Li, W. Xin, J. Zhu and Y. Luo, Matte waterborne polyurethane fabric nanocoating with versatility via monolayered montmorillonite nanosheets, *Prog. Org. Coat.*, 2021, **159**, 106420.
5 F. Bauer, U. Decker, S. Naumov and C. Riedel, UV curing and matting of acrylate nanocomposite coatings by 172nm excimer irradiation, Part 2, *Prog. Org. Coat.*, 2010, **3**(69), 287–293.
6 X. Yan, Y. Han and T. Yin, Synthesis of Urea-Formaldehyde Microcapsule Containing Fluororesin and Its Effect on Performances of Waterborne Coatings on Wood Surface, *Polymers*, 2021, **11**(13), 1674.
7 X. Yan and L. Wang, Preparation of Shellac Resin Microcapsules Coated with Urea Formaldehyde Resin and Properties of Waterborne Paint Films for Tilia amurensis Rupr, *Membranes*, 2020, **10**(10), 278.

8 Q. W. Yong, D. Xu, Q. Liu, Y. Xiao and D. D. Wei, Advances in polymer-based matte coatings: A review, *Polym. Adv. Technol.*, 2022, **1**(33), 5–19.

9 Y. Meng, P. Lv, Q. Liu, B. Liao, H. Pang and W. Liu, Preparation and characterization of soybean oil-based waterborne polyurethane/acrylate hybrid emulsions for self-matting coatings, *New J. Chem.*, 2019, **48**(43), 19193–19199.

10 Y. C. Du, S. L. Shi, C. Y. Bu, H. X. Dai, Z. G. Guo and G. Y. Tang, Effect of Particle Size Distribution of Calcined Diatomites on the Extinction Performance, *Part. Sci. Technol.*, 2011, **4**(29), 368–377.

11 Q. Yong, F. Nian, B. Liao, Y. Guo, L. Huang, L. Wang and H. Pang, Synthesis and surface analysis of self-matt coating based on waterborne polyurethane resin and study on the matt mechanism, *Polym. Bull.*, 2016, **4**(74), 1061–1076.

12 Z. Ding, J. Li, W. Xin, G. Zhang and Y. Luo, Low gloss waterborne polyurethane coatings with anti-dripping and flame retardancy via montmorillonite nanosheets, *Prog. Org. Coat.*, 2019, **136**, 105273.

13 S. S. Lee, J. H. Koo, S. S. Lee, S. G. Chai and J. C. Lim, Gloss reduction in low temperature curable hybrid powder coatings, *Prog. Org. Coat.*, 2003, **4**(46), 266–272.

14 S. Bhattarai, S.-I. Lee, D.-S. Lee and Y.-S. Lee, Effect of Molecular Weight of Poly(tetramethylene glycol) on Waterborne Polyurethane Dispersion Coating Gloss, *Bull. Korean Chem. Soc.*, 2019, **10**(40), 1046–1049.

15 Q. Liu, B. Liao, H. Pang, M. Lu and Y. Meng, Preparation and characterization of a self -matting coating based on waterborne polyurethane-polyacrylate hybrid dispersions, *Prog. Org. Coat.*, 2020, **143**, 105551.

16 Y. Meng, Q. Yong, B. Liao, W. Zeng and H. Pang, Synthesis, characterization and formation mechanism of acrylate emulsion-based self-matting coatings, *New J. Chem.*, 2020, **33**(44), 13971–13978.

17 J. Chang, X. Wang, J. Shao, X. Li, W. Xin and Y. Luo, Synthesis and Characterization of Environmentally-Friendly Self-Matting Waterborne Polyurethane Coatings, *Coatings*, 2020, **5**(10), 494.

18 Z. Sun, H. Fan, Y. Chen and J. Huang, Synthesis of self-matting waterborne polyurethane coatings with excellent transmittance, *Polym. Int.*, 2018, **1**(67), 78–84.

19 R. Schubert, F. Frost, M. Hinkefuss, R. Konieczny, B. Marquardt, R. Mehnert and M. R. Buchmeiser, VUV-induced micro-folding of acrylate-based coatings 2. Characterization of surface properties, *Surf. Coat. Technol.*, 2009, **24**(203), 3734–3740.

20 R. Schubert, T. Scherzer, M. Hinkefuss, B. Marquardt, J. Vogel and M. R. Buchmeiser, VUV-induced micro-folding of acrylate-based coatings 1. Real-time methods for the determination of the micro-folding kinetics, *Surf. Coat. Technol.*, 2009, **13**(203), 1844–1849.

21 F. Bauer, U. Decker, K. Czihal, R. Mehnert, C. Riedel, M. Riemschneider, R. Schubert and M. R. Buchmeiser, UV curing and matting of acrylate nanocomposite coatings by 172nm excimer irradiation, *Prog. Org. Coat.*, 2009, **4**(64), 474–481.

22 D. Chandra and A. J. Crosby, Self-wrinkling of UV-cured polymer films, *Adv. Mater.*, 2011, **30**(23), 3441–3445.

23 J. Lacombe and C. Soulie-Ziakovic, Controlling self-patterning of acrylate films by photopolymerization, *Polym. Chem.*, 2017, **7**(8), 1129–1137.

24 X. Xiong, Q. Ma, Y. Yuan, Z. Wu and M. Zhang, Current situation and key manufacturing considerations of green furniture in China: A review, *J. Cleaner Prod.*, 2020, **267**, 121957.

25 Y. Qi, L. Shen, J. Zhang, J. Yao, R. Lu and T. Miyakoshi, Species and release characteristics of VOCs in furniture coating process, *Environ. Pollut.*, 2019, **245**, 810–819.

26 Y. Cai, Y. Wu, L. Yang, F. Yang, Y. Wang and T. Cheng, A wood sponge sensor for heavy metal ion detection and adsorption, *Wood Sci. Technol.*, 2022, **4**(56), 1175–1190.

27 Y. Su, S. Zhang, Y. Chen, T. Yuan and Z. Yang, One-step synthesis of novel renewable multi-functional linseed oil-based acrylate prepolymers and its application in UV-curable coatings, *Prog. Org. Coat.*, 2020, **148**, 105820.

28 J. Aizpurua, L. Martin, M. Fernández, A. González and L. Irusta, Recyclable, remendable and healing polyurethane/acrylic coatings from UV curable waterborne dispersions containing Diels-Alder moieties, *Prog. Org. Coat.*, 2020, **139**, 105460.

29 X. Li, D. Wang, L. Zhao, X. Hou, L. Liu, B. Feng, M. Li, P. Zheng, X. Zhao and S. Wei, UV LED curable epoxy soybean-oil-based waterborne PUA resin for wood coatings, *Prog. Org. Coat.*, 2021, **151**, 105942.

30 X. Yan, Y. Chang and X. Qian, The Properties of an Aluminum/UV-Curable, Infrared, Low-Emissivity Coating Modified by Nano-Silica Slurry, *Coatings*, 2020, **4**(10), 382.

31 X. Yan and L. Wang, Preparation and Performance of a Waterborne UV/Al Low Infrared Emissivity Coating, *Appl. Sci.*, 2020, **18**(10), 6423.

32 F. Bauer, U. Decker, S. Naumov and C. Riedel, Photoinitiator-free UV curing and matting of acrylate-based nanocomposite coatings: Part 3, *Prog. Org. Coat.*, 2014, **6**(77), 1085–1094.

33 D. D. Wei, X. M. Huang, J. J. Zeng, S. L. Deng and J. H. Xu, Facile synthesis of a castor oil-based hyperbranched acrylate oligomer and its application in UV-curable coatings, *J. Appl. Polym. Sci.*, 2020, **36**(137), 49054.

34 C. Esposito Corcione and M. Frigione, Factors influencing photo curing kinetics of novel UV-cured siloxane-modified acrylic coatings: Oxygen inhibition and composition, *Thermochim. Acta*, 2012, **534**, 21–27.

35 J.-W. Park, K.-B. Sim, G.-S. Shim, J.-H. Back, D. Baek, H.-J. Kim and S. Shin, Depth profile of thin coating through surface and interfacial cutting analysis of UV curing system, *Mater. Des.*, 2019, **178**, 107855.

36 Y. F. Yun, Y. Guan and Y. J. Zhang, Patterned PHEMA Films Synthesized by Redox Polymerization for Multicellular Spheroid Generation, *Ind. Eng. Chem. Res.*, 2019, **25**(58), 10713–10723.

37 F. Bauer, R. Flyunt, K. Czihal, H. Langguth, R. Mehmert, R. S. Chubert and M. R. Buchmeiser, UV curing and

matting of acrylate coatings reinforced by nano-silica and micro-corundum particles, *Prog. Org. Coat.*, 2007, **2**(60), 121–126.

38 Z. Yang, J. Wu, G. Ma, C. Hou, Y. Niu, H. Duan and X. Hao, Effect of the particle sizes of silica on the properties of UV-curing matting coatings, *J. Coat. Technol. Res.*, 2021, **1**(18), 183–192.

39 Q. Yong, F. Nian, B. Liao, L. Huang, L. Wang and H. Pang, Synthesis and characterization of solvent-free waterborne polyurethane dispersion with both sulfonic and carboxylic hydrophilic chain-extending agents for matt coating applications, *RSC Adv.*, 2015, **130**(5), 107413–107420.

40 J. H. Chen, K. M. Peng and W. P. Tu, Novel waterborne UV-curable coatings based on hyperbranched polymers via electrophoretic deposition, *RSC Adv.*, 2019, **20**(9), 11013–11025.

41 Z. Lin, Z. Sun, C. Xu, A. Zhang, J. Xiang and H. Fan, A self-matting waterborne polyurethane coating with admirable abrasion-resistance, *RSC Adv.*, 2021, **44**(11), 27620–27626.

42 Q. Yong, H. Pang, B. Liao, W. Mo, F. Huang, H. Huang and Y. Zhao, Preparation and characterization of low gloss aqueous coating via forming self-roughed surface based on waterborne polyurethane acrylate hybrid emulsion, *Prog. Org. Coat.*, 2018, **115**, 18–26.

43 L. Wang and X. Yan, Mechanical and Optical Properties of Thermochromic Reversible Waterborne Primer Film on Tilia europaea with 1,2-Benzo-6-diethylaminofluorane Based Microcapsules, *Polymers*, 2020, **9**(12), 2062.

44 J. B. Bergmann, D. Moatsou, V. A. Surapaneni, M. Thielen, T. Speck, B. D. Wilts and U. Steiner, Polymerization-Induced Wrinkled Surfaces with Controlled Topography as Slippery Surfaces for Colorado Potato Beetles, *Adv. Mater. Interfaces*, 2020, **12**(7), 2000129.

45 M. Henke, B. Lis and T. Krystofiak, Gloss Level of HDF Finished with Different Numbers of Layers and Hardened with UV Hg-Ga Lamps of Selected Power, *Coatings*, 2022, **4**(12), 533.

46 H. Lee, S. Chae, A. Yi and H. J. Kim, Hydrophobic stretchable polydimethylsiloxane films with wrinkle patterns prepared via a metal-assisted chemical etching process using a Si master mold, *J. Appl. Polym. Sci.*, 2021, **19**(138), 50398.

47 Y. Wu, X. Wu, F. Yang and J. Ye, Preparation and Characterization of Waterborne UV Lacquer Product Modified by Zinc Oxide with Flower Shape, *Polymers*, 2020, **3**(12), 668.

48 X. Wu, F. Yang, J. Gan, W. Zhao and Y. Wu, A flower-like waterborne coating with self-cleaning, self-repairing properties for superhydrophobic applications, *J. Mater. Res. Technol.*, 2021, (14), 1820–1829.

49 X. Wu, F. Yang, J. Gan, Z. Kong and Y. Wu, A Superhydrophobic, Antibacterial, and Durable Surface of Poplar Wood, *Nanomaterials*, 2021, **8**(11), 1185.

50 X. Yang, J. Su, J. Xiong and H. Wang, Preparation of Nano-silica with Radial Wrinkle Structures for Self-cleaning and Superhydrophobic Coatings, *Fibers Polym.*, 2022, **5**(23), 1293–1299.

51 M. Byeon, S. K. Cho, M. S. Um, J. H. Lee, E. S. Kim and W. J. Choi, Enhancing Hydrophobicity of Polymer Thin Film-Coated Surface by Wrinkling Method, *Macromol. Res.*, 2020, **12**(28), 1104–1110.

52 Q. Zhang, C. Huang, H. Wang, M. Hu, H. Li and X. Liu, UV-curable coating crosslinked by a novel hyperbranched polyurethane acrylate with excellent mechanical properties and hardness, *RSC Adv.*, 2016, **109**(6), 107942–107950.

53 C. Yuan, J. Wang, M. Cui and Y. Peng, Aqueous PUA emulsion prepared by dispersing polyurethane prepolymer in polyacrylate emulsion, *J. Appl. Polym. Sci.*, 2016, **11**(133), 43203.

54 B. Liang, J. Zhao, G. Li, Y. K. Huang, Z. H. Yang and T. Yuan, Facile synthesis and characterization of novel multi-functional bio-based acrylate prepolymers derived from tung oil and its application in UV-curable coatings, *Ind. Crops Prod.*, 2019, **138**, 111585.

55 R. V. Sheril, M. Mariatti and P. Samayamutthirian, Single and hybrid mineral fillers (talc/silica and talc/calcium carbonate)-filled polypropylene composites: Effects of filler loading and ratios, *J. Vinyl Addit. Technol.*, 2014, **3**(20), 160–167.